Biochemical Pharmacology 78 (2009) 1127–1138

Contents lists available at ScienceDirect

Biochemical Pharmacology

journal homepage: www.elsevier.com/locate/biochempharm

Retinoid metabolism and ALDH1A2 (RALDH2) expression are altered in the transgenic adenocarcinoma mouse prostate model

Sue Ellen Touma [a], Sven Perner [b], Mark A. Rubin [b], David M. Nanus [c,d], Lorraine J. Gudas [a,d,*]

[a] Department of Pharmacology, Weill Cornell Medical College of Cornell University, 1300 York Avenue, New York, NY 10065, United States
[b] Department of Pathology, Weill Cornell Medical College of Cornell University, 1300 York Avenue, New York, NY 10065, United States
[c] Division of Hematology/Oncology, Department of Medicine, Weill Cornell Medical College of Cornell University, 1300 York Avenue, New York, NY 10065, United States
[d] Department of Urology, Weill Cornell Medical College of Cornell University, 1300 York Avenue, New York, NY 10065, United States

ARTICLE INFO

Article history:
Received 18 March 2009
Accepted 16 June 2009

Keywords:
Human prostate cancer
TRAMP
Retinoic acid
Epithelial cells
Carcinogenesis

ABSTRACT

Retinoids, which include vitamin A (retinol) and metabolites such as retinoic acid, can inhibit tumor growth and reverse carcinogenesis in animal models of prostate cancer. We analyzed retinoid signaling and metabolism in the TRAMP (transgenic adenocarcinoma mouse prostate) model. We detected increased retinol and retinyl esters in prostates pooled from 24 to 36 week TRAMP transgenic positive mice compared to nontransgenic littermates by HPLC. We used quantitative RT-PCR to measure transcripts for genes involved in retinoid signaling and metabolism, including ALDH1A1, ALDH1A2, ALDH1A3, CYP26A1, LRAT, and RARβ_2, in prostate tissue from TRAMP positive (+) and age-matched littermate control mice ranging from 18 to 36 weeks. Transcript levels of ALDH1A1, a putative stem cell marker, were decreased in ventral and lateral lobes of prostates from TRAMP mice compared to age-matched, nontransgenic mice. ALDH1A2 (RALDH2) mRNA levels in dorsal and anterior lobes of TRAMP+ mice were lower than in age-matched (24 week) nontransgenic mice. We detected lower RARβ_2 mRNA levels in dorsal prostate lobes of 36 week TRAMP mice relative to nontransgenic mice. We detected high levels of ALDH1A2 protein in the cytoplasm and nucleus in nontransgenic murine prostate paraffin sections, and lower ALDH1A2 protein levels in all prostate lobes of TRAMP mice compared to nontransgenic mice by immunohistochemistry. We also detected much lower cytoplasmic ALDH1A2 protein levels in all human prostate cancer paraffin sections stained (19 total) relative to normal human prostate tissue on the same sections. Our data indicate that this reduction in ALDH1A2 protein is an early event in human prostate cancer.

1. Introduction

Prostate cancer is the most common cancer among men, accounting for approximately 28,660 deaths (10% of cancer related deaths) [1]. It is estimated that 186,320 new cases will be diagnosed this year [1]. Retinol (vitamin A) and its derivatives, such as retinoic acid (RA), known collectively as retinoids, have been shown to reverse hyperplasia in carcinogen-induced prostate cancer mouse models [2–4]. These effects are due to the regulation retinoids exert on cell growth and differentiation [5].

While RA has been effective in cancer chemoprevention, abnormal changes in retinoid sensitivity and metabolism occur during tumor development. Many studies have shown a reduction in retinoic acid receptor β_2 (RARβ_2) expression in prostate cancer relative to normal tissue, resulting in part from aberrant histone acetylation and promoter DNA methylation [6–8]. Our laboratory has shown that the levels of LRAT (lecithin:retinol acyltransferase), the primary enzyme responsible for the metabolism of retinol to retinyl esters, are reduced in human prostate cancer, with an associated decrease of retinoid levels in tissues [9]. Retinyl esters serve as the storage form of retinol in the liver and in other tissues in the body. Another report has shown RA levels to be five to eight times lower in human prostate cancer tissues as compared to normal prostate [10].

Pharmacologic inhibition of DNA methyltransferase 1 (DNMT1) and subsequent expression profiling identified the epigenetic silencing of ALDH1A2 in human prostate cancer [11]. ALDH1A2 (Gene ID: 19378) belongs to the aldehyde dehydrogenase (ALDH)

Abbreviations: AP, anterior prostate; CYP26A1, cytochrome p450 hydroxylase family 26 A1; DP, dorsal prostate; HPLC, high pressure liquid chromatography; LP, lateral prostate; LRAT, lecithin:retinol acyltransferase; PBS, phosphate buffered saline; RA, all-*trans* retinoic acid; RALDH, retinaldehyde dehydrogenase; RAR, retinoic acid receptor; RARα, retinoic acid receptor alpha; RARβ, retinoic acid receptor beta; RARγ, retinoic acid receptor gamma; RXR, retinoid X receptor; SV40, simian virus 40; Tag, T antigen; TRAMP, transgenic adenocarcinoma mouse prostate; VP, ventral prostate; WT, wild type.

* Corresponding author at: 1300 York Avenue, Rm. E-409, New York, NY 10065, United States. Tel.: +1 212 746 6250; fax: +1 212 746 8858.
E-mail address: ljgudas@med.cornell.edu (L.J. Gudas).

0006-2952/$ – see front matter © 2009 Elsevier Inc. All rights reserved.
doi:10.1016/j.bcp.2009.06.022

enzyme family, also known as retinaldehyde dehydrogenases (RALDHs), that catalyzes the irreversible oxidation of all-*trans* retinaldehyde to all-*trans* RA, following the reversible conversion of all-*trans* retinol to all-*trans* retinaldehyde [12]. There are three ALDH1A subtypes: ALDH1A1, ALDH1A2, and ALDH1A3, which differ in substrate specificity and tissue localization [13]. ALDH1A1 has also been reported to be a stem cell marker [14]. ALDH1A2 (mRNA and protein) is expressed in a few adult tissues, primarily in the urogenital tract, while it is highly expressed in the mouse embryo trunk and cervical regions [15]. An ALDH1A2 (Raldh2$^{-/-}$) knockout mouse has a host of developmental abnormalities resulting from severe RA deficiency [16]. In addition to the potential role of ALDH1A2 as a tumor suppressor [11], the alterations in ALDH enzyme expression in prostate cancer suggest that these enzymes may contribute to abnormal retinoid levels during carcinogenesis. For example, reduced ALDH1A1–3 mRNA levels in the androgen-responsive LNCaP prostate cancer cell line have been reported [17].

It is not known when alterations in retinoid signaling and metabolism occur during carcinogenesis. The use of mouse models of cancer, such as the TRAMP model, can facilitate a better understanding of the order of events that contribute to human cancer development. The TRAMP (transgenic adenocarcinoma mouse prostate) transgene consists of an androgen regulated, prostate specific probasin promoter driving the expression of SV40 T and t antigen gene expression [18,19]. The TRAMP model is a well characterized model that displays disease progression similar to human prostate cancer, making it an attractive model to study all stages of prostate cancer [20–26]. In particular, the TRAMP model has been useful in both testing prostate cancer chemopreventive treatments [27–34] and in understanding resistance to hormone therapy [35]. In another mouse model of prostate cancer, the Lady transgenic model, the carotenoid lycopene was shown to reduce the incidence of prostate cancer [36].

The mouse prostate is composed for four distinct lobes: ventral (VP), lateral (LP), dorsal (DP), and anterior (AP; also known as coagulating gland) [20]. The human prostate consists of a central, transition, and peripheral zone [37]. Comparative microarray studies confirmed previous observations, indicating that the dorsal/lateral lobes (often pooled together as a dorsolateral lobe) are most related to the peripheral zone of the human prostate, the most frequent site of human prostate cancer [37,38]. Consistent with findings in human prostate cancer, microarray analysis has revealed a decrease in ALDH1A1 mRNA levels in prostate tissue from TRAMP mice as compared to normal mice [17,39]. Treatment with retinoic acid was shown to induce apoptosis and inhibit cancer progression in both the TRAMP-derived C2N cell line and in TRAMP mice [40]. These results, along with the reduction of ALDH1A expression in human prostate cancer [11], led us to examine retinoid metabolism during the carcinogenesis process in the TRAMP model. Understanding the role of retinoid signaling during prostate carcinogenesis will lead to improved detection and chemoprevention strategies and to the development of novel therapies for prostate cancer.

2. Materials and methods

2.1. Transgenic animals

All animals were housed and maintained in the Research Animal Resource Center at Weill Cornell Medical College and all procedures were performed according to the animal protocol approved by the Institutional Animal Care and Use Committee (IACUC). A TRAMP C57BL/6 male expressing the rat probasin promoter-SV40 large T-antigen transgene (PB-Tag) was purchased from The Jackson Laboratory (Bar Harbor, ME) and bred with wild type nontransgenic C57BL/6 females. Mouse tail DNA isolation and PCR based genotype screening of all offspring were performed as described [18].

2.2. Tissue preparation for protein/RNA analyses

TRAMP mice used in these studies were hemizygous for the probasin promoter-SV40 large T-antigen transgene (PB-Tag). Nontransgenic littermate males served as negative controls for all experiments. For all experiments, prostate tissues were taken from three transgenic and nontransgenic mice at each time point: 18, 24, and 30–36 weeks of age. Mice were sacrificed by cervical dislocation, the urogenital tract (seminal vesicles, bladder and prostate lobes) was removed, and prostate lobes were microdissected and processed separately. For Western/immunohistochemical analyses, the urogenital tract was placed in about 20 ml PBS plus 1 Complete Mini Protease Inhibitor Cocktail tablet (Roche Applied Science, Indianapolis, IN). Each lobe was cut in half and was further prepared for either Western or immunohistochemical procedures. Tissues for Western blotting were flash frozen in liquid nitrogen and homogenized directly in denaturing 2% sodium dodecyl sulfate (SDS) sample buffer. For immunohistochemistry, tissues were fixed in 4% paraformaldehyde overnight at 4 °C and then transferred to 70% ethanol for tissue processing and paraffin embedding. For RNA isolation, microdissection of prostate lobes was performed in RNA*later* solution (Ambion, Austin, TX) to submerge the urogenital tract. Prostate lobes were stored in aliquots of RNA*later* overnight at 4 °C and then transferred to −20 °C until RNA extraction was performed.

2.3. RNA extraction and quantitative RT-PCR

Total RNA was isolated from prostate tissues using the RNeasy Mini Kit (Qiagen, Valencia, CA) according to the manufacturer's instructions. SuperScript™ II reverse transcriptase (Invitrogen, Carlsbad, CA) was used to carry out reverse transcription of 1–5 μg RNA. Dilution of cDNA products was performed according to the amount of RNA reverse-transcribed (1:5 for 1 μg RNA, 1:12.5 for 2.5 μg RNA, and 1:25 for 5 μg RNA). All primer pairs were designed to span an intron in order to eliminate any contribution from genomic DNA contamination. Primer sequences are located in Table 1. Real time PCR was carried out using the Bio-Rad MyiQ Single-Color Real-Time PCR Detection System (Bio-Rad, Hercules, CA). Each 20 μl PCR reaction was composed of 10 μl iQ SYBR Green Supermix (Bio-Rad), 1 μl forward primer (5 μM), 1 μl reverse

Table 1
Primer sequences used for quantitative RT-PCR.

Gene		Primer sequence (5′–3′)	Product size (bp)
ALDH1A1	Forward	CTCCTCTCACGGCTCTTCAC	289
	Reverse	CCATGGTGTGCAAACTCAAC	
ALDH1A2	Forward	ATGGGTGAGTTTGGCTTACG	274
	Reverse	GGTTCATTGGAAGGCAGAAA	
ALDH1A3	Forward	AGTGTGGAGTTCGCCAAGAAGAGG	193
	Reverse	AGACCGTGGGTTTGATGAACAGCC	
RARβ$_2$[a]	Forward	GATCCTGGATTTCTACACCG	247
	Reverse	CACTGACGCCATAGTGGTA	
CYP26A1[a]	Forward	GAAACATTGCAGATGGTGCTTCAG	272
	Reverse	CGGCTGAAGGCCTGCATAATCAC	
LRAT	Forward	GACTTACTGCAGATATGGCTCTCG	176
	Reverse	ATGGGATACAGATTGCAGGAAGGG	
36B4[a]	Forward	AGAACAACCCAGCTCTGGAGAAA	448
	Reverse	ACACCCTCCAGAAAGCGAGAGT	

[a] Primers sequences were obtained from [41].

primer (5 μM), 6 μl H_2O, and 2 μl diluted cDNA. PCR reactions were run according to the following steps: initial denaturation of template/activation of polymerase at 95 °C for 3 min, and then 50 cycles of (1) denaturation at 94 °C for 20 s, (2) annealing at 60 °C for 45 s, (3) extension at 72 °C for 45 s, and (4) fluorescence measurement at 84 °C. Threshold cycle (C_T) values were calculated by MyIQ software (Bio-Rad) and displayed a linear relationship with relative cDNA input. Relative expression levels were calculated using the Genex Microsoft Excel macro (Bio-Rad) with normalization to the ribosomal phosphoprotein 36B4 mRNA [41]. Triplicate reactions for each cDNA sample were prepared with similar results. As a negative control, reactions were set up using water instead of template. PCR products for each primer pair were sequenced to ensure primer specificity.

2.4. Retinoid extraction and quantitation by HPLC

Prostate tissues were dissected along with lung and liver tissues from nontransgenic and transgenic TRAMP males (6 mice/group). Individual lobes were microdissected and pooled from two mice to have sufficient tissue for retinoid extraction and detection by HPLC. The retinoid extraction/HPLC separation procedures have been previously described [9]. Tissues were weighed and homogenized in 500 μl cold PBS with an electric homogenizer (Ultra-Turrax T8, Ika, Wilmington, NC). Retinyl acetate (25 μL of 100 μM stock, Sigma–Aldrich, St. Louis, MO) was added to each sample as an internal control for extraction efficiency. Retinoids were extracted by adding 350 μl of organic solution (acetonitrile/butanol, 50:50, v/v) followed by 300 μl of saturated K_2HPO_4. Samples were centrifuged for 10 min at 14,000 rpm at room temperature to separate the retinoid-containing organic phase from the remaining nonorganic components. High pressure liquid chromatography (HPLC) was performed using a Waters Millenium system. Each sample (100 μl of the 350 μl) was loaded onto an analytical 5-μm reverse phase C_{18} column (Vydac, Hesperia, CA) and eluted at a flow rate of 1.5 ml/min. Retinoid levels were calculated using known standards and peak area detected at 340 nm. The levels of retinol and retinyl esters were normalized to tissue weight and retinyl acetate to control for extraction efficiency.

2.5. ALDH1A2 polyclonal antibody generation

A rabbit anti-mouse ALDH1A2 polyclonal antibody was generated by contract with Alpha Diagnostics International (San Antonio, TX). Two peptides of the mouse ALDH1A2 protein (NP_033048), TGEQVCEVQEADKVDIDK (aa # 43–60) and CSPNIIFADADLDYAVEQAH (aa # 272–290), were selected for antibody production based on optimal antigenicity, accessibility, and hydrophilicity profiles. These peptide sequences are conserved in mouse and human ALDH1A2 (Genbank NCBI). Rabbits were immunized with a mixture of both peptides. Sera from 2 immunized rabbits (# 10221 and 10222) were pooled and subjected to affinity chromatography for polyclonal antibody purification in July, 2006.

By performing blocking experiments with 20-fold excess of each of the two peptides individually prior to immunohistochemistry, we showed that the peptide to aa # 272–290 can block almost all of the immunostaining with the ALDH1A2 polyclonal antibody; both nuclear and cytoplasmic staining were greatly reduced in WT murine prostate paraffin sections and the human prostate sections in the presence of the peptide aa # 272–290. In contrast, 20-fold excess of the peptide to aa # 43–60 did not completely block the immunostaining with the ALDH1A2 antibody in WT murine prostate sections or in the human prostate sections (data not shown).

2.6. Western blotting

Prostate tissue extracts (15–30 μg protein/sample) were separated on 10% (for ALDH1A2) or 18% (for S100A4) SDS-PAGE gels and proteins were transferred to nitrocellulose membranes (catalog #162-0091, Bio-Rad, Hercules, CA) by electroblotting. The membranes were stained with Ponceau S (Sigma, St. Louis, MO) to confirm proper transfer and equal loading. ALDH1A2 was detected using a 1:250 dilution of the rabbit polyclonal antibody (Alpha Diagnostics International, San Antonio, TX). S100A4 was detected using a 1:250 dilution of the rabbit anit-human S100A4 polyclonal antibody (catalog # A5114, Dako, Carpinteria, CA). An actin polyclonal antibody (1:500 dilution, catalog # sc-1616; Santa Cruz Biotechnology, Santa Cruz, CA) was used as a loading control. Membranes were blocked for 1 h in PBS containing 5% Blotto (catalog # sc-2325, Santa Cruz Biotechnology, Santa Cruz, CA) and 0.1% Tween 20 (Sigma–Aldrich) at room temperature. Primary antibody incubation was performed overnight at 4 °C in PBS containing 5% Blotto and 0.1% Tween 20. After a 1 h incubation with an IgG horseradish peroxidase (HRP) conjugated secondary antibody at room temperature (anti-rabbit for ALDH1A2 and S100A4, 1:5000 dilution, catalog # sc-2054; anti-goat for actin, 1:5000 dilution; catalog # sc-2020, Santa Cruz Biotechnology), the membranes were developed with Supersignal Substrate (Pierce, Rockford, IL) for 5 min and exposed to Biomax film (Eastman Kodak, Rochester, NY). Secondary antibodies were diluted in PBS containing 5% Blotto and 0.1% Tween 20.

2.7. Immunohistochemistry

Prostate tissues from TRAMP mice were prepared as described above. Human prostate tissue specimens were obtained by the Department of Pathology and the Urological Oncology Division at New York Presbyterian Hospital–Weill Cornell Medical Center. To confirm ALDH1A2 antibody specificity, wild type and ALDH1A2 (Raldh2$^{-/-}$) embryos (E12/13) were provided for immunohistochemical staining as a generous gift from Dr. Karen Niederreither. Embryos were fixed in 4% paraformaldehyde overnight and then transferred to 70% ethanol for tissue processing and paraffin embedding. Sections were deparaffinized in Histo-Clear (National Diagnostics, Atlanta, GA), followed by rehydration in a graded series of ethanol. Antigen retrieval was performed by heat with Antigen Unmasking Solution (high pH, catalog # H-3301, Vector Laboratories, Burlingame, CA) in a pressure cooker for 2 min. A 3% solution of H_2O_2 in 100% methanol was used to quench the endogenous peroxidase activity (15 min incubation). Slides were subsequently stained using the Rabbit SuperPicTure Kit (Invitrogen, Carlsbad, CA). Primary antibody incubation was performed with affinity-purified, polyclonal rabbit anti-mouse ALDH1A2 primary antibody (Alpha Diagnostics International, San Antonio, TX) diluted 1:125 in 1.5% goat serum in PBS. Adjacent sections for mouse and human tissue samples were also stained with a 1:500 dilution of rabbit anti-human S100A4 (catalog # A5114, Dako, Carpinteria, CA) antibody in 1.5% goat serum. Primary antibody incubation was performed overnight at 4 °C in a humidified chamber. Secondary antibody incubation was then performed with 150 μl of horseradish peroxidase conjugated goat anti-rabbit secondary antibody for 1 h at room temperature (antibody provided in the kit-diluted 1:1 with PBS before use). Color was developed using 3,3′-diaminobenzidine chromogen substrate, followed by counterstaining with hematoxylin (Vector, Burlingame, CA). As a negative control, preimmune serum was used in place of primary antibody.

Table 2
Pathological scores of human prostate tumor specimens.

Gleason grade	Number of patients (19 total adenocarcinomas)	Pathologic stage			
		T2A	T2B	T2C	T3B
6	6 (32%)	1	1	4	0
7	11 (58%)	0	0	10	1
8	1 (5%)	0	0	1	0
9	1 (5%)	0	0	0	1

2.8. Human prostate cancer tissue specimens

Nineteen prostate cancer cases were obtained from the Department of Pathology and Laboratory Medicine at the Weill Medical College of Cornell University/New York Presbyterian Hospital. An Institutional Review Board approved protocol allowed for tissue procurement. Gleason scores and tumor stage information for the human prostate tumor specimens used in this study are located in Table 2.

2.9. Evaluation of immunohistochemical staining and pathology

ALDH1A2 and S100A4 protein expression and prostate cancer pathology were assessed by two pathologists (MAR and SP) in the Department of Pathology and Laboratory Medicine, Weill Cornell Medical College/New York Presbyterian Hospital. The pathology was also evaluated according to the published criteria established for the TRAMP model [20,37].

2.10. Microscope image acquisition

Pictures of immunohistochemical staining and histology were taken using the Nikon NIS Elements Advanced Research (version 2.3) imaging software (Nikon, Melville, NY) and DS-Fi1 color camera (Nikon, Melville, NY) connected to the Nikon Eclipse TE2000-E inverted microscope (Nikon, Melville, NY). The Nikon NIS Elements Advanced Research imaging software settings for image acquisition are as follows: exposure—manual, light intensity—4.0 V, gain—1.00×, contrast—high, exposure time for 100× magnification—3–4 ms, exposure time for 200× magnification—8 ms, exposure time for 400× magnification—30 ms and exposure time for 600× magnification—60 ms. The auto white balance action was performed once prior to image acquisition to adjust background color.

2.11. Statistical analysis

A two-tailed Student's t test was used to assess statistical significance between groups for quantitative RT-PCR, HPLC, and Western blotting analyses. TRAMP mice were compared to age-matched littermate controls. Statistical significance was designated as follows: $p \leq 0.05$(*).

3. Results

3.1. Measurement of prostate tissue retinoid levels in TRAMP mice

Since retinoid levels have been shown to be reduced in human prostate cancer tissues and cell lines as compared to normal tissue, we were interested in measuring retinoid levels in prostate tissues from nontransgenic age-matched littermate control mice (designated as WT) and TRAMP mice [9,10]. Retinoids were extracted from the four mouse prostate lobes, ventral (VP), lateral (LP), dorsal (DP), and anterior (AP), and measured by reverse phase high pressure liquid chromatography (HPLC). Prostates were pooled from 2 mice for a total of 3 samples each from 6 TRAMP transgenic negative and 6 TRAMP positive mice (designated as TRAMP) ranging from 24 to 36 weeks of age. Retinol was not detected in any of the wild type controls (Fig. 1, indicated by‡). In contrast, retinol could be detected in all lobes of the TRAMP mice, with levels of 0.08 ± 0.0 pmol/mg, 0.15 ± 0.1 pmol/mg, 0.07 ± 0.0 pmol/mg, and 0.06 ± 0.0 pmol/mg in the VP, LP, DP, and AP, respectively. Although very low, retinyl esters could be detected in all lobes of wild type mice, except the LP (indicated by §), with levels of 0.02 ± 0.0 pmol/mg in the VP, 0.02 ± 0.0 pmol/mg in the DP, and 0.06 ± 0.0 pmol/mg in the AP (Fig. 1). Retinyl ester levels were higher in the TRAMP prostate tissues than in littermate nontransgenic control tissue (Fig. 1). The LP and DP of TRAMP mice displayed the highest retinyl ester levels, 0.11 ± 0.0 pmol/mg and 0.19 ± 0.0 pmol/mg, as compared to the VP (0.02 ± 0.0 pmol/mg) and AP (0.04 ± 0.0 pmol/mg) (Fig. 1). In summary, the prostate lobes from TRAMP mice showed statistically significant increases in retinol levels as compared to the WT control mice ($p \leq 0.05$). The retinyl ester levels in the LP and the DP of TRAMP mice were increased relative to levels in the littermate nontransgenic control tissue (WT) (Fig. 1). Levels of retinyl esters in the AP of TRAMP mice were lower than in the AP of WT mice (Fig. 1). RA and retinaldehyde were not detected in all tissues tested (data not shown), indicating that the concentrations were below our detection level for the number of mouse prostate lobes analyzed per sample in these experiments.

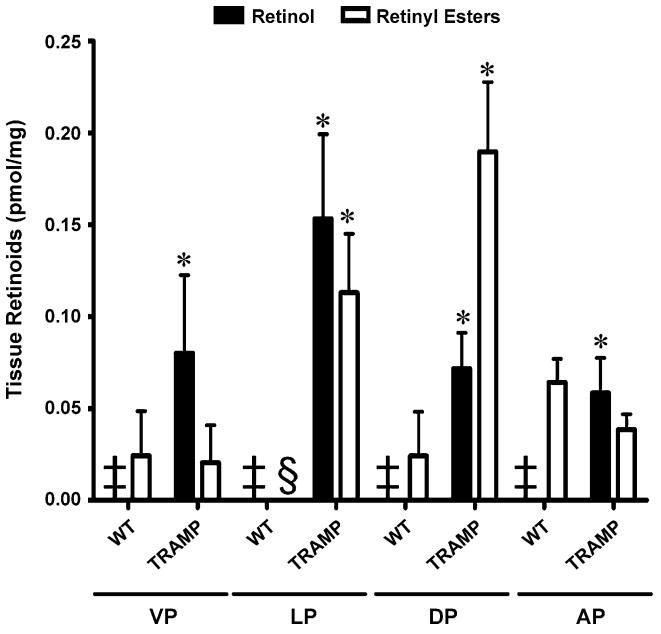

Fig. 1. Altered retinoid levels in TRAMP mice. Retinoids were extracted from prostate tissues of TRAMP(+) and age-matched nontransgenic littermate control mice ranging from 24 to 36 weeks of age (6/group) and were separated by reverse-phase HPLC analysis. Individual prostate lobes from 2 mice were pooled together for the retinoid extraction, giving a total of 3 samples each for control, non-transgenic littermate (designated WT) and TRAMP. Retinol (white) and retinyl ester (black) levels (pmol/mg tissue) in prostate tissue were calculated using known standards and normalization to prostate tissue weight. Comparisons for statistical significance were made between the WT and the TRAMP mice within each lobe for each type of retinoid. Error bars = standard error. VP, ventral prostate; LP, lateral prostate; DP, dorsal prostate; and AP, anterior prostate. ‡, retinol was not detected. §, retinyl esters were not detected. *$p \leq 0.05$ as determined by two-tailed Student's t test, comparing TRAMP mice to their age-matched littermate controls (TRAMP = TRAMP+, i.e. containing the transgene).

3.2. Expression profiles of genes involved in retinoid metabolism

HPLC analysis measures retinoid levels. We were also interested in assessing the expression of several genes involved in main-

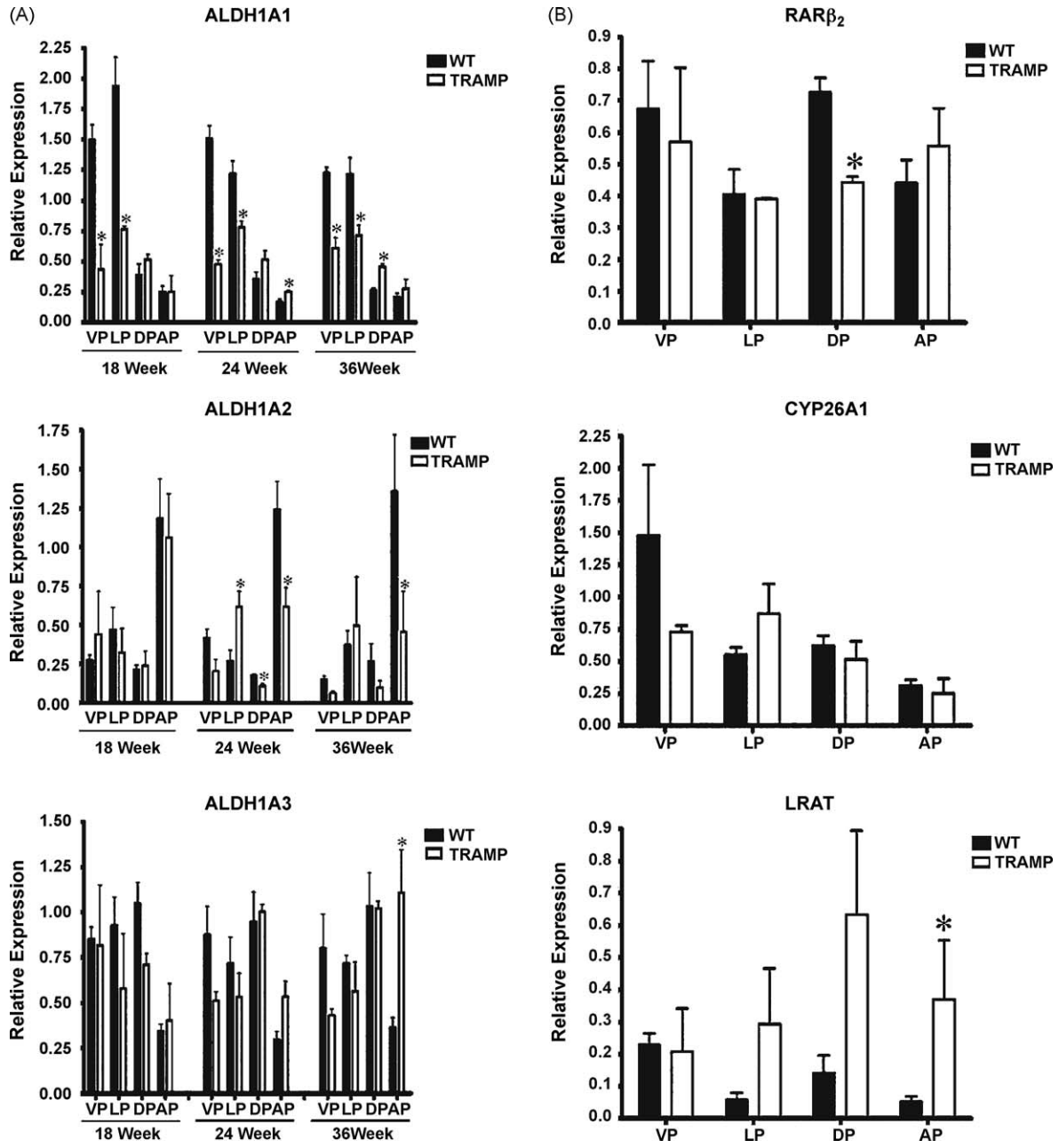

Fig. 2. Relative ALDH1A1–3, RARβ$_2$, CYP26A1, and LRAT mRNA levels by quantitative RT-PCR in prostate tissue from normal and TRAMP mice. (A) Total RNA was extracted and reverse-transcribed from prostate lobes microdissected from three nontransgenic mice at 18, 24, and 36 weeks of age. The bars indicate the average transcript levels of ALDH1A1, ALDH1A2, and ALDH1A3 in prostate tissue from age-matched nontransgenic controls (WT, black bars) and TRAMP (white bars) normalized to 36B4 mRNA levels in each sample. (B) Relative mRNA levels of RARβ$_2$, CYP26A1, and LRAT measured by quantitative RT-PCR in WT (black bars) and TRAMP mice (white bars) at 36 weeks of age. All samples were normalized to 36B4. VP, ventral prostate; LP, lateral prostate; DP, dorsal prostate; and AP, anterior prostate. Relative expression was calculated using the Bio-Rad Genex software, where all prostate lobes from a given age group were processed independently. Error bars = standard error. Comparisons for statistical analysis were made for each lobe between the WT and the TRAMP mice at each of the time points. $^*p \leq 0.05$ as determined by two-tailed Student's t test, comparing TRAMP mice to their age-matched littermate controls (TRAMP = TRAMP+).

taining normal retinoid metabolism and the changes that may occur during prostate cancer development. Quantitative RT-PCR was used to measure the levels of ALDH1A1, ALDH1A2, and ALDH1A3 mRNAs in prostate lobes from three nontransgenic age-matched littermate control mice (WT) and three TRAMP transgenic positive mice at 18, 24, and 36 weeks of age (Fig. 2A). Relative mRNA levels for all genes tested were normalized to the ribosomal phosphoprotein 36B4 mRNA. The relative mRNA levels of ALDH1A1, ALDH1A2, and ALDH1A3 in the VP, LP, DP, and AP of wild type mice at 18, 24, and 36 weeks of age indicated no age related changes in nontransgenic mice, as the expression trends were similar at all three ages tested (Fig. 2A).

ALDH1A1 mRNA levels were highest in the VP and LP, and were approximately five times lower in both the DP and AP in WT mice at all ages tested (Fig. 2A). ALDH1A1 mRNA levels were lower in the VP and LP from TRAMP mice than in age-matched littermate controls at all three ages tested (Fig. 2A). In contrast, TRAMP ALDH1A1 mRNA levels were moderately higher in the AP at 24 weeks and the DP at 36 weeks relative to those in WT (Fig. 2A).

In nontransgenic mice (WT), ALDH1A2 mRNA levels were the highest in the AP, and about five times lower in the VP, LP, and DP at all ages tested (Fig. 2A). ALDH1A2 mRNA levels were lower in the DP and AP of TRAMP mice compared to WT mice at 24 and 36 weeks (Fig. 2A). In contrast, ALDH1A2 mRNA levels in the LP of

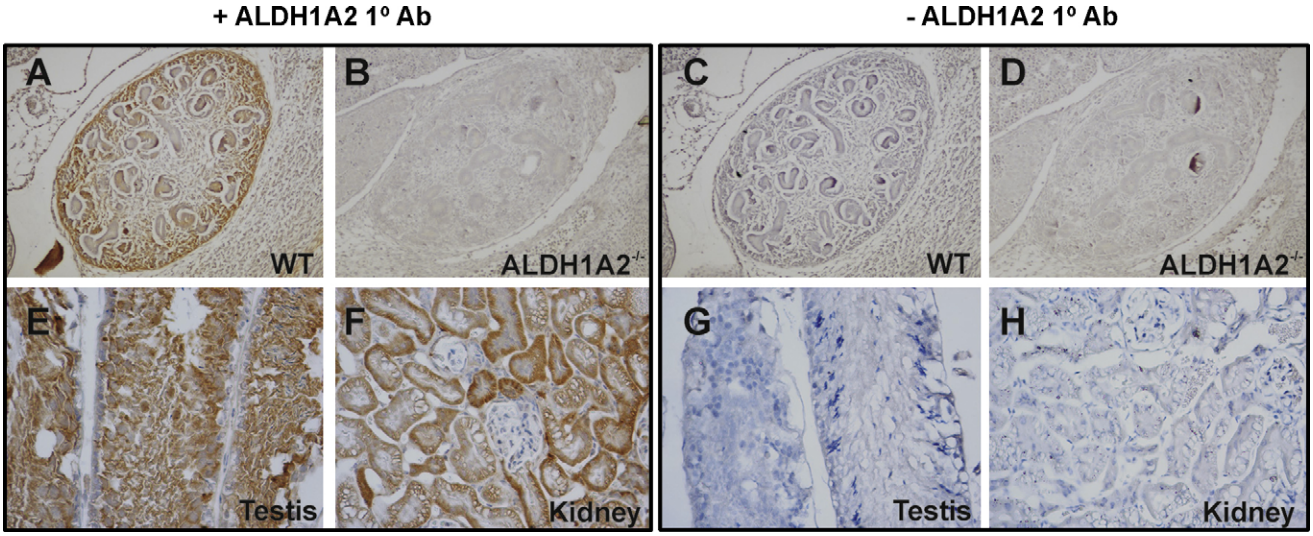

Fig. 3. ALDH1A2 protein in wild type and ALDH1A2$^{-/-}$ (Raldh2 $^{-/-}$) embryos and adult mouse tissues. (A) Wild type mouse embryo at E12/13 (WT). ALDH1A2 staining located in the metanephros. (B) ALDH1A2$^{-/-}$ embryo at E12/13. No ALDH1A2 staining was observed in the metanephros, confirming antibody specificity. (E) Wild type mouse testis at 36 weeks of age. ALDH1A2 staining located in the germ cells but not in the spermatagonia. (F) Wild type mouse kidney at 36 weeks of age. ALDH1A2 staining was observed in the tubular cells, but not in the glomeruli. (C, D, G and H) Negative control incubated with preimmune serum instead of primary antibody. (A–D) 200× magnification. (E and H) 400× magnification.

TRAMP mice were similar to or higher than to those in the nontransgenic (WT) mice (Fig. 2A).

ALDH1A3 mRNA transcript levels were lowest in the AP of WT mice as compared to the other three lobes, a trend opposite to that found with ALDH1A2 mRNA (Fig. 2A). The differences in mean ALDH1A3 mRNA levels between TRAMP and WT mice were generally not statistically significant, except in the AP at 36 weeks (Fig. 2A).

LRAT esterifies retinol into retinyl esters and CYP26A1 oxidizes RA into more polar metabolites [5]. The expression of both genes serves as an indicator of their respective actions in the retinoid metabolism pathway. Thus, we compared the mRNA levels of CYP26A1, and LRAT in WT versus TRAMP murine prostates. For CYP26A1, the highest mRNA levels were found in the VP of WT mice, with comparable lower levels in the other three lobes in nontransgenic (WT) mice (Fig. 2B). We observed no statistically significant changes in CYP26A1 mRNA levels in TRAMP mice as compared to the nontransgenic littermate controls (Fig. 2B). LRAT mRNA levels are relatively higher in the VP as compared to the other lobes in nontransgenic (WT) mice (Fig. 2B). This pattern of LRAT mRNA expression differs in the TRAMP mice (Fig. 2B).

We also examined RARβ_2 expression, as it is a retinoic acid receptor that is involved in regulating cell growth and differentiation and its expression is silenced in prostate cancer [5]. Lower RARβ_2 transcript levels were only observed in the DP of TRAMP mice compared to WT mice (Fig. 2B). Thus, although RARβ_2, CYP26A1, and LRAT mRNA levels are regulated by retinoic acid [5], these mRNAs do not exhibit similar patterns of expression in the different prostate lobes of TRAMP mice.

3.3. ALDH1A2 protein levels in nontransgenic and TRAMP prostate tissues

The reduction in ALDH1A2 mRNA levels in the DP and AP of TRAMP mice relative to nontransgenic control mice (Fig. 2A) is consistent with a previous report that ALDH1A2 expression is reduced in human prostate cancer [11]. In order to assess ALDH1A2 protein levels in the TRAMP model, our laboratory generated a rabbit polyclonal anti-mouse ALDH1A2 antibody that is specific for the ALDH1A2 isoform and displays cross-reactivity with other species, including human. The specificity of the ALDH1A2 antibody was tested using immunohistochemical staining of WT mouse embryos and ALDH1A2$^{-/-}$ (Raldh2$^{-/-}$) E12/13 mutant embryos [16,42]. Using the ALDH1A2 antibody generated by our laboratory, staining in the metanephros and renal cortex in WT embryos was seen (Fig. 3A), but no staining was seen in the ALDH1A2 mutant embryos (Fig. 3B). Incubation of samples without primary antibody resulted in no signal in both WT and mutant embryos (Fig. 3C and D). Thus, our ALDH1A2 antibody is specific for immunostaining under the conditions we used (Fig. 3). Previous immunohistochemical staining by other researchers using another ALDH1A2 specific antibody also resulted in positive staining in the metanephros (embryonic kidney) and renal cortex in wild type mouse embryos at day 14.5 [43].

Immunohistochemical staining on adult mouse testis and kidney tissues served as positive controls for ALDH1A2 staining (Fig. 3E and F). The testis expresses high levels of ALDH1A2 protein as detected by Western blot analysis [43]. ALDH1A2 transcripts were specifically detected in the germ cells of the testis, but not in the spermatagonia [44]. We observed specific ALDH1A2 localization to the germ cells (Fig. 3E). The kidney has been found to express ALDH1A2 protein by both Western and immunohistochemical methods [45]. We detected ALDH1A2 protein in kidney tubular cells, but not in the glomeruli (Fig. 3F). ALDH1A2 protein was only observed in the cytoplasm of both tissue types tested (Fig. 3). Incubation of these testis and kidney samples without primary antibody resulted in no signal in both WT and mutant embryos (Fig. 3G and H).

We then examined ALDH1A2 protein levels by Western blot analysis in prostate extracts from TRAMP mice at 18–36 weeks and compared the levels with age-matched, littermate transgenic negative controls. A Western blot of DP tissue from 18 to 36 week old nontransgenic and TRAMP mice incubated with ALDH1A2 and S100A4 antibodies, along with the appropriate positive controls (testis for ALDH1A2; PC3 human prostate cancer cell extract for S100A4, see below) is shown as a representative blot (Fig. 4A; for quantitation of similar blots, Fig. 4C). There is a reduced level of ALDH1A2 protein in one TRAMP sample at 24 weeks and in all three TRAMP DP samples at 36 weeks. These data confirm the trends observed at the mRNA level for ALDH1A2 in the DP lobe

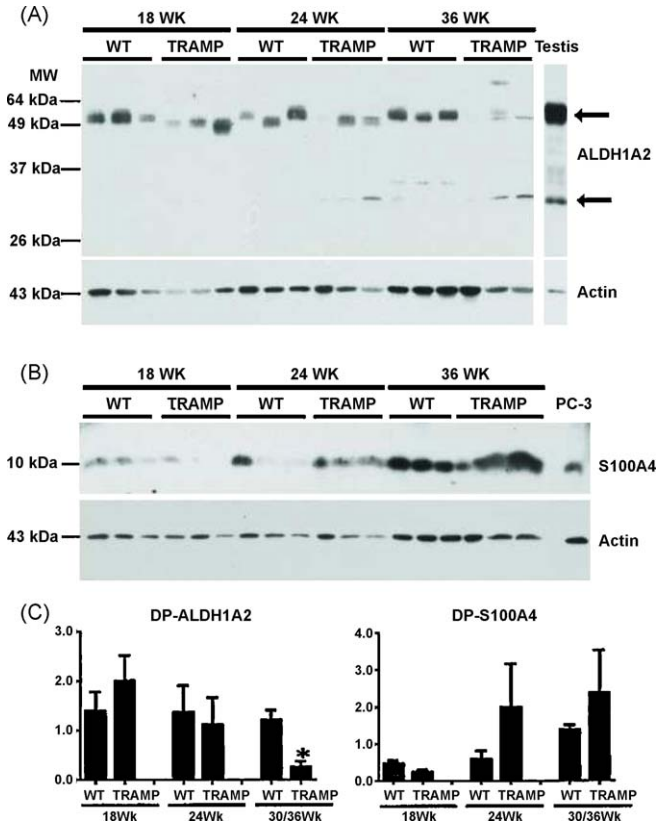

Fig. 4. ALDH1A2 and S100A4 western blot analyses. Tissue extracts were obtained from microdissected dorsal prostate lobes (30 μg protein loaded/lane) from nontransgenic (labeled as WT) littermate controls and TRAMP mice at 18, 24, and 36 weeks of age (3 mice per condition). (A) Western blot analysis performed with the polyclonal rabbit anti-mouse ALDH1A2 antibody. (B) Western blot analysis performed with the polyclonal rabbit anti-human S100A4 antibody. For a loading control, these blots were stripped and reblotted with a polyclonal goat anti-human actin antibody. Positive controls: ALDH1A2-wild type testis extract (15 μg protein loaded/lane); S100A4-PC3 cell extract (30 μg protein loaded/lane). This experiment was performed three times with similar results; one blot is shown. The upper arrow at the right in panel A shows ALDH1A2; the lower arrow points to the non-specific protein band at ~30 kDa. (C) Densitometric quantitation of similar ALDH1A2 and S100A4 Western Blots. Band density was measured using the Fluor Chem 8800 software (Alpha Innotech) for the bands from ALDH1A2 (left) and S100A4 (right). Western blots normalized to actin for all prostate samples. Error bars = standard error. *$p \leq 0.05$ as determined by two-tailed Student's t test. TRAMP mice were compared to age-matched littermate nontransgenic controls (WT). DP, dorsal prostate.

(Fig. 2A). However, ALDH1A2 protein levels did not show any significant changes in the VP, LP, and AP lobes of TRAMP mice versus the age-matched controls (data not shown). These ALDH1A2 protein results do not reflect the reduced ALDH1A2 mRNA levels observed in the AP lobe or the increased mRNA levels in the LP of TRAMP mice (Fig. 2A), potentially indicating regulatory differences with respect to ALDH1A2 at the RNA versus the protein level. Additional bands around 30 kDa were detected in the testis extract control and in some mouse prostate extracts (Fig. 4A).

We also measured the levels of a known tumor marker, S100A4, also known as fibroblast specific protein 1 (FSP1), a calcium-binding protein that is overexpressed during the progression of prostate cancer in the TRAMP model [46]. S100A4 is normally expressed in fibroblast cells and regulates cell growth and signaling. S100A4 expression is increased in the TRAMP prostate tissue as compared to age-matched controls, indicating its potential as a marker to monitor prostate cancer progression in the TRAMP model [46]. However, we observed increases in S100A4 protein levels in both the nontransgenic control mice and in TRAMP mice over time (Fig. 4B). S100A4 protein levels increased with age when comparing the TRAMP mice of different ages (Fig. 4B). The TRAMP mice had ~2-fold higher S100A4 protein levels than WT mice after normalization to actin protein levels (Fig. 4B and C).

3.4. ALDH1A2 protein expression in nontransgenic and TRAMP prostate tissue: immunohistochemical analysis

We also analyzed ALDH1A2 and S100A4 protein levels and location by immunohistochemistry. We observed ALDH1A2 in both the nucleus and the cytoplasm in *all nontransgenic* adult murine prostate lobes (DP and LP shown as examples in Fig. 5A and C; VP and AP-data not shown). As expected, S100A4 expression is confined to the fibroblast cells of the thin stromal layer surrounding each prostate gland (DP and LP shown as examples in Fig. 5B and D; VP and AP-data not shown).

Immunohistochemical analysis of a tumor in the DP in a 36 week old TRAMP mouse indicates that the cancer cells have lost the nuclear localization seen in nontransgenic prostate epithelial cells and only exhibit a weak ALDH1A2 cytoplasmic stain (Fig. 5E see arrow; similar results for VP and AP-data not shown). The lower ALDH1A2 signal in the cancer cells of the DP is consistent with the lower ALDH1A2 mRNA (Fig. 2A) and protein levels observed in the DP by Western analysis (Fig. 4). No ALDH1A2 staining was detected in the stroma of these tumors in the DP (Fig. 5E see arrow). Competition of the ALDH1A2 antibody with the peptide to which the antibody was generated resulted in a major reduction in signal (Fig. 5K and L). S100A4 staining is increased in the DP of TRAMP mice relative to normal nontransgenic mice. S100A4 displays a punctate stain throughout the glandular and stromal compartments (Fig. 5F).

Immunohistochemical analysis of a tumor in the LP of the same 36 week old TRAMP mouse shows that the cancer cells have lost the nuclear localization of ALDH1A2 but still show weak cytoplasmic stain (Fig. 5G, black arrow). In contrast to the DP, in the LP there is an increase in ALDH1A2 staining in the thickened stromal layer surrounding the prostate cancer cells in a 36 week old TRAMP mouse (Fig. 5G, white arrow). The staining of S100A4 is also increased in the LP tumor relative to normal nontransgenic mice, with stromal localization as well as invasion into the prostate gland (Fig. 5H).

3.5. ALDH1A2 protein expression in human prostate cancer specimens

Sections of human prostate adenocarcinomas (n = 19) were also stained with the same ALDH1A2 and S100A4 antibodies. We obtained prostate cancer tumor tissue varying in Gleason scores with the following distribution: grade 6 (32%), grade 7 (58%), grade 8 (5%), and grade 9 (5%) (see Table 2 for additional details on tumor stage of human adenocarcinomas used in this study). The human tumors were from the peripheral, transitional, or central zones of the prostate, depending on where the tumors were found. ALDH1A2 protein was observed in both basal and luminal cells of normal human prostate glands (Fig. 6A, B, E and F, see white arrow, luminal; black arrow, basal cells). For most benign glands, ALDH1A2 staining was stronger in the basal cells than luminal cells (see magnified area in Fig. 6B and F). ALDH1A2 protein expression in the human prostate gland was detected mainly in the cytoplasmic compartment of cells.

There was little to no ALDH1A2 protein in the human prostate cancer cells (see magnified area in Fig. 6B and F, see red arrow). All nineteen cases contained prostate cancer adjacent to normal benign glands on the same section and displayed reduced ALDH1A2 staining in cancer tissue as compared to the benign tissue. S100A4 protein was detected in the normal gland (Fig. 6C, D,

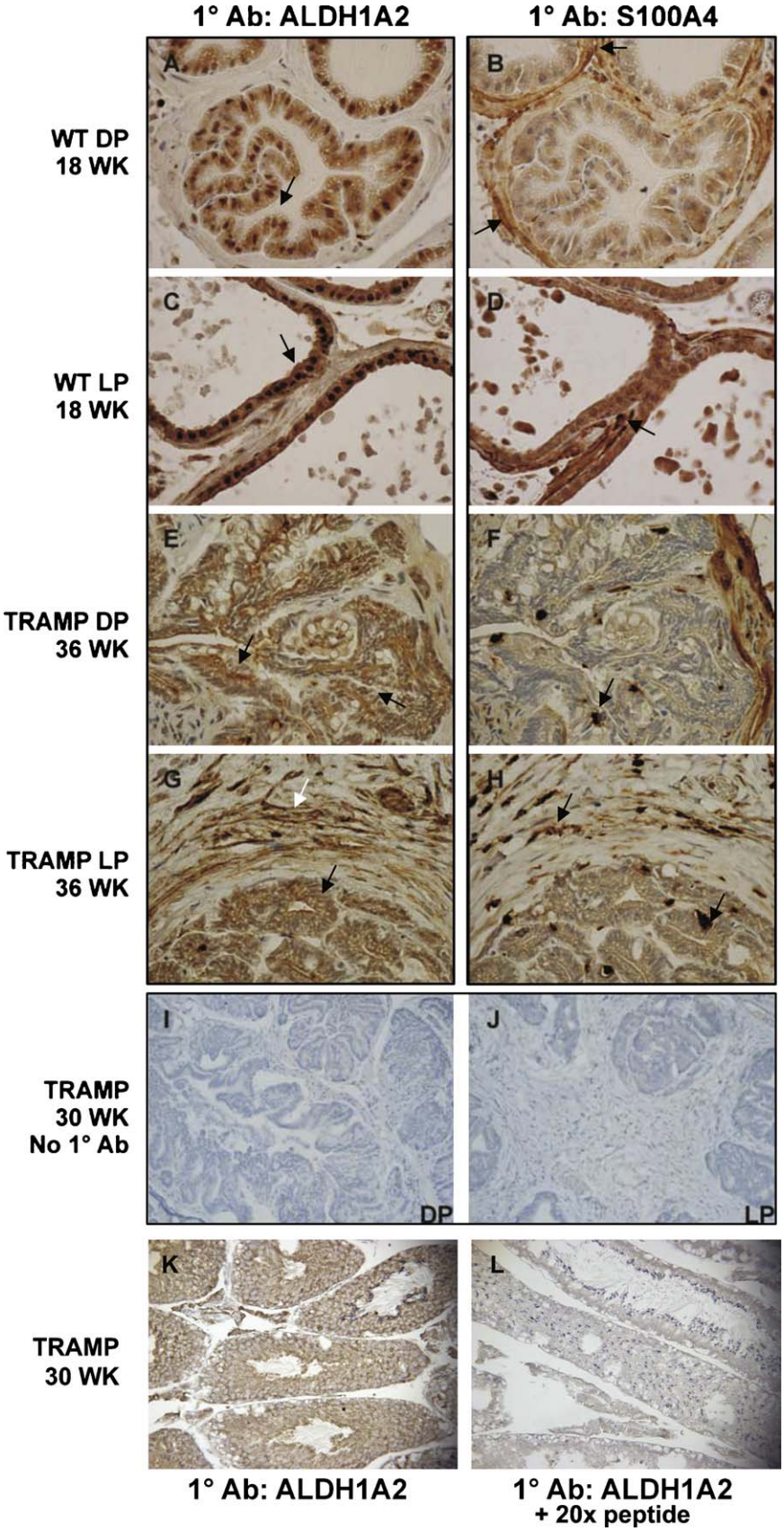

Fig. 5. ALDH1A2 and S100A4 protein expression in nontransgenic mouse and TRAMP prostate tissue. All tissue sections were stained with hematoxylin (blue). (A, C, E, and G) ALDH1A2 staining. (B, D, F, and H) S100A4 staining. (A–H) 600× magnification. Dorsal lobe (A) and lateral lobe (C) from an 18 week old nontransgenic mouse. Strong nuclear and cytoplasmic ALDH1A2 staining (brown stain) representative of normal prostate epithelial cells in all lobes. S100A4 (brown stain) staining in fibroblast cells surrounding a normal prostate gland in dorsal lobe (B) and lateral lobe (D). (E) Dorsal prostate tumor tissue in a 36 week old TRAMP mouse, showing weak cytoplasmic ALDH1A2 staining in prostate cancer cells with little to no stain in the nuclei. There is no ALDH1A2 staining in the stroma of dorsal prostate tissue in the TRAMP mouse. (F) S100A4 staining in the

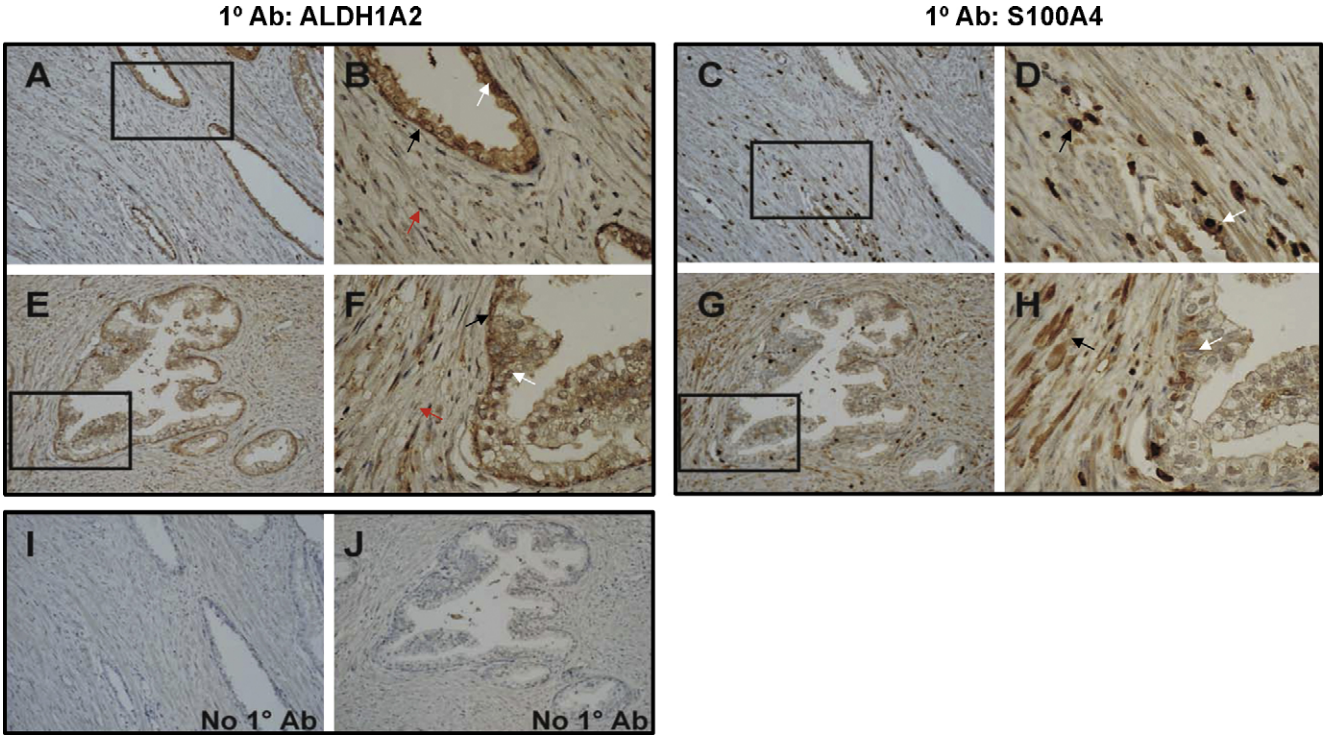

Fig. 6. ALDH1A2 and S100A4 protein expression in human prostate specimens. (A–J) Representative slides of a human prostate tumor tissue. (A, B, E and F) ALDH1A2 staining at 200× and 600× (boxed areas of A and E) magnification. (B and F) ALDH1A2 staining located in the cytoplasmic compartment of basal and luminal cells in a normal prostate gland with weak staining in adjacent cancer cells. (C, D, G and H) S100A4 staining at 200× and 600× (boxed areas of C and G) magnification. S100A4 staining is seen in benign glands, as well as in surrounding stroma. (I and J) Negative controls, prostate specimens incubated with preimmune serum instead of primary antibody, 200× magnification (arrows indicate areas on sections discussed in the Section 3).

G and H, white arrow) and expression was increased around the malignant tissue (Fig. 6C, D, G and H, black arrow).

4. Discussion

Previous studies examining ALDH1A1–3 expression in prostate cancer were performed in DU145 and LNCaP cancer cell lines and human prostate cancer tissue, all of which represent advanced stages of prostate cancer [11,17]. In this study, we utilized the TRAMP model to assess retinoid signaling and metabolism (see Fig. 7) at various stages of prostate cancer. When considering the relevance of lobe-specific expression changes in the TRAMP model to human disease, it is important to consider the established similarity of the peripheral zone, the predominant site of human prostate cancer, to the dorsal and lateral lobes in the mouse prostate [37,38,47].

4.1. Altered retinoid metabolism in prostate cancer tissue from TRAMP mice

In a previous report by our laboratory, retinol and retinyl ester levels were reduced in human prostate cancer cell lines relative to cultured normal human prostate epithelial cells [9]. In addition, LRAT protein expression was reduced in these cell lines and in human prostate cancer specimens as compared to normal human prostate tissue [9]. The human LRAT promoter is also more active in cultured normal human prostate epithelial cells than in cultured human prostate carcinoma lines [48]. This decrease in LRAT expression has also been observed in other studies from our laboratory with human kidney, breast, skin and oral cavity cancers relative to normal cells [49,50].

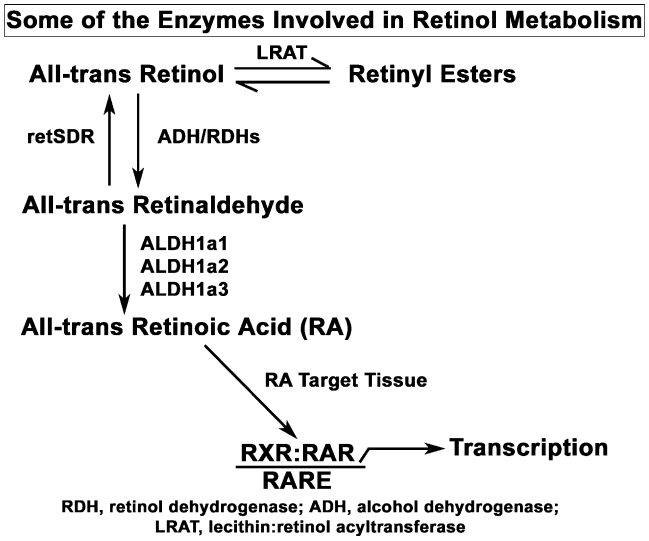

Fig. 7. The Role of ALDH1a2 in retinoic acid synthesis.

stroma of TRAMP mice and among prostate cancer cells within the gland. (G) Lateral prostate tumor tissue in a 36 week old TRAMP mouse. The ALDH1A2 staining pattern in the prostate cancer cells is similar to (E). Positive staining of ALDH1A2 in the lateral prostate stroma, which is unique to this lobe. (F) S100A4 staining in the prostate cancer and lateral prostate stroma. (I–J) Negative controls incubated with preimmune serum instead of primary antibody. (I) Prostate tumor tissue from dorsal prostate of 30 week old TRAMP mouse, 200× magnification. (J) Prostate tumor tissue from lateral prostate of 30 week old TRAMP mouse, 200× magnification. (K) ALDH1A2 staining of prostate tumor tissue from 30 week old TRAMP mouse, 200× magnification. (L) Adjacent section of ALDH1A2 staining of prostate tumor tissue from 30 week old TRAMP mouse. Tumor tissue section was simultaneously incubated with the 20× peptides to which the antibody was generated (arrows indicate areas of sections discussed in the Section 3). (For interpretation of the references to color in this figure legend, the reader is referred to the web version of the article.)

In this study, we measured higher levels of retinol and retinyl esters in the TRAMP mice as compared to nontransgenic mice (Fig. 1). Although the TRAMP model represents many features of human prostate cancer development, SV40 can induce gene expression that may or may not be relevant to the human disease [51,52]. SV40 is used to induce artificially murine prostate cancer since mice do not spontaneously develop prostate cancer [53]. In the report by Guo et al., LRAT expression and retinoid metabolism were also assessed in the SV40-immortalized human prostate epithelial cell lines pRNS-1-1 and in the ras overexpressing pRNS-1-1/ras line [9,54]. The metabolism of retinol and retinyl esters was lower in both the pRNS-1-1 and pRNS-1-1/ras cell lines as compared to the cultured untransformed, normal human prostate epithelial cells (PrEC), but was higher than that in the human prostate cancer cell lines, including LNCaP and PC-3 [9]. Since we were not able to measure retinol and retinyl esters directly in human prostate cancer tissues in our prior research, we cannot directly compare the HPLC data from TRAMP mice (Fig. 1) to the data from human cell lines and paraffin sections [9]. However, the retinyl ester levels in the TRAMP tumors may be difficult to compare to normal mouse prostate (Fig. 1) because normal mouse prostate contains several different types of cells, whereas the TRAMP tumor tissue is more homogeneous. If some of the cell types in the normal prostate, such as fibroblasts, do not express LRAT, then this would reduce the retinyl ester level measured in the normal prostate relative to that in the TRAMP tumor tissue, which is primarily epithelial. The reason for this is that the data in Fig. 1 are expressed/tissue weight. This could explain the apparent discrepancy between the higher retinyl ester levels seen in the TRAMP mice compared to WT mice (Fig. 1) and the lower LRAT protein levels seen in human prostate cancer specimens as compared to normal human prostate specimens [9].

4.2. The expression of ALDH1A1–3 is altered in human cancers

The loss of ALDH1A enzymes can negatively impact retinoid metabolism and signaling that occurs during carcinogenesis. ALDH1A1–3 transcripts have been shown to be reduced in human prostate cancer [11,17]. ALDH1A2 protein was also not detected in human prostate cancer compared to normal human prostate tissue by immunohistochemistry [11]. All-*trans* retinaldehyde is the major substrate for ALDH1A2. In addition, a catalytically inactive and N-terminally truncated transcript of ALDH1A2, named RALDH2-T, was highly expressed in T-cell acute lymphoblastic leukemia (T-ALL) cell lines [55]. ALDH1A3 mRNA and protein were not detected in MCF-7 breast cancer cells and this was associated with impaired retinoid metabolism in those cells [56]. Reactivation of ALDH1A3 mRNA expression in the AGS gastric cancer cell line was achieved with 5-aza-2′-deoxycytidine treatment, potentially indicating a promoter methylation-induced mechanism of ALDH1A3 gene silencing in this gastric cancer cell line [57]. ALDH1A2 mRNA levels in DU145 prostate cancer cells could also be increased with 5-aza-2′-deoxycytidine treatment [11]. All of these findings are significant because they link aberrant or reduced expression of various members of the ALDH family of enzymes with human cancer.

Increased ALDH1A1 expression is associated with malignant tumors in the breast [58]. Both normal and cancer stem cells exhibit high ALDH1A1 protein expression and enzyme activity [14]. It is possible that increased ALDH1A1 expression within a pre-malignant stem cell population contributes to neoplastic transformation of these stem cells and the establishment of a cancer stem cell phenotype [14]. Putative prostate stem cells have been characterized in normal human and prostate cancer tissue [59]. Also, putative prostate stem cell populations have been characterized in wild type mice and in the TRAMP model [60–62]. We show that the ALDH1A1 mRNA levels were decreased in the ventral and lateral lobes of TRAMP mice at 18, 24, and 36 weeks, while mRNA levels increased in the anterior and dorsal lobes at 24 and 36 weeks, respectively, relative to age-matched nontransgenic mice (Fig. 2A). These results show that lobe-specific differences in ALDH1A1 expression exist in TRAMP mice relative to nontransgenic mice. Changes in ALDH1A1 mRNA levels in prostates from TRAMP versus nontransgenic control mice could indicate the relative abundance of cancer stem cells in these tissues.

4.3. Reduced ALDH1A2 mRNA and protein in prostate cancer tissue from TRAMP mice

By Western blot analysis, we observed a large reduction (about 4-fold relative to actin) in ALDH1A2 protein in the DP tissues in all three 36 week old TRAMP mice compared to age-matched nontransgenic littermate mice (Fig. 4A and C). In contrast, no changes in ALDH1A2 protein levels were detected by Western blot analysis in the VP, LP, or AP lobes of TRAMP mice versus age-matched controls (data not shown). The presence of multiple protein bands on the ALDH1A2 Western blot raises the question of alternative ALDH1A2 transcripts (Fig. 4). Currently, only one transcript has been identified for the mouse ALDH1A2 (gene: NM_009022; protein: NP_033048), but three transcript variants have been identified for human ALDH1A2. Human ALDH1A2 isoform 1 (gene: NM_003888; protein: NP_003879) represents the full length protein, while ALDH1A2 isoform 2 (gene: NM_170696; protein: NP_733797) lacks an internal exon. ALDH1A2 isoform 3 (gene: 170697; NP_733798) contains a distinct 5′-untranslated region and a truncated N-terminus compared to isoforms 1 and 2. ALDH1A2 isoform 3 is also known as RALDH2-T, mentioned previously as the N-terminally truncated transcript expressed in T-ALL cell lines [55]. Since the full length mouse and human ALDH1A2 genes share approximately 98% homology (determined by NCBI BLAST), it is likely that similar transcript variants are present in the mouse. Additional bands around 30 kDa were detected in some nontransgenic and TRAMP prostate tissue samples, suggesting that our ALDH1A2 antibody is also detecting potential prostate tissue specific isoforms (Fig. 4). Based on the peptide sequences used to generate the ALDH1A2 antibody, it is expected that the antibody we used would detect all three human isoforms and should cross-react with any mouse variants homologous to the human isoforms.

Immunohistochemical staining revealed that ALDH1A2 protein expression is reduced in the prostate cancer cells of *all* lobes from TRAMP mice. The ALDH1A2 protein shows a weak cytoplasmic stain and loss of the nuclear stain in the prostate cancer cells (DP and LP shown in Fig. 5E and G; VP and AP-data not shown). The staining pattern of ALDH1A2 protein in the normal mouse prostate epithelial cells is similar in all lobes, with strong staining in both the nuclei and cytoplasm (DP and LP shown in Fig. 5A and C; VP and AP-data not shown).

Review of the slides with respect to stromal staining of ALDH1A2 in the different lobes has shown positive staining for ALDH1A2 *only* in the stroma of the LP in TRAMP mice (Fig. 5H). ALDH1A2 protein expression in the LP stroma (Fig. 5H) could account for the increased mRNA levels observed in TRAMP mice at 24 weeks (Fig. 2A). Our immunohistochemical staining results (Fig. 5) did not totally reflect the results from quantitative RT-PCR or Western blot analyses, possibly because changes in ALDH1A2 protein levels and in the location of expression are associated with increasing tumor volume over time in the TRAMP model.

4.4. Reduced ALDH1A2 protein in human prostate cancer tissue

A loss of ALDH1A2 protein expression was also observed in human prostate cancer specimens as compared to adjacent benign

tissue (Fig. 6A, B, E and F). There was no gradient of ALDH1A2 staining that correlated with the varying stages of prostate cancer included within the sample set tested. Staining was present in the normal glands and absent in all malignant tissue. In normal glands, strong ALDH1A2 staining was observed in the basal cell layer, but ALDH1A2 staining was also present in the luminal cells (Fig. 6A, B, E and F). The localization of ALDH1A2 protein to both the basal and luminal cells of normal human prostate epithelial cells is consistent with the comparable ALDH1A2 mRNA levels in basal and luminal cells detected by microarray analysis of sorted normal human prostate epithelial cells (GEO record GDS1973) [63]. Little to no ALDH1A2 staining was detected in the human prostate cancer cells (Fig. 6A, B, E and F). As with the TRAMP mouse model data (Fig. 5), ALDH1A2 protein expression was either present in the benign glands or weak to absent in human prostate cancer tissue (Fig. 6). These results are also consistent with the report that the retinoid X receptor (RXRα) and LRAT display a more intense expression in the basal layer as compared to the luminal cells of benign human prostate glands [9,64].

We do not understand why ALDH1A2 is expressed both in the cytoplasm and nucleus of all normal mouse prostate epithelial cells (Fig. 5A and C), but is only expressed in the cytoplasm of normal human prostate epithelial cells (Fig. 6). The nuclear localization of ALDH1A2 protein in mouse prostate epithelial cells may be explained by the fact that the organization of the mouse and human prostates are different [37,65]. Although similarities in expression profiles exist between the peripheral zone of the human prostate and the dorsal/lateral mouse prostate lobe, there are also differences in gene expression among normal human and mouse prostates that may account for the difference in ALDH1A2 cellular localization [38].

We also utilized the LOCATE mammalian subcellular localization database to determine the predicted localization of the known ALDH1A2 human and mouse proteins [66]. All three ALDH1A2 human isoforms were predicted primarily to have a cytoplasmic localization, with a 12–14.5% possibility of localization to both the cytoplasm and nucleus, based on their peptide sequences. The localization of the mouse ALDH1A2 protein was also predicted to be in the cytoplasm, with about a 14% possibility to be located in the peroxisomes or the plasma membrane. Based on these analyses and the similarity of human and mouse ALDH1A2 proteins, ALDH1A2 should be predominantly found in the cytoplasm. Despite the differences in ALDH1A2 localization in normal cells, we observed a reduction in ALDH1A2 protein levels in prostate cancer cells when compared to normal prostate epithelial cells in both the TRAMP model (Fig. 5) and human prostate cancer specimens (Fig. 6).

Since various mouse models recapitulate different aspects of prostate cancer, ALDH1A family gene expression, retinoid metabolism, and retinoid signaling should be examined in other transgenic and knockout mouse models of prostate cancer to extend the results obtained in this study [52,67]. Identifying a reduction or loss of ALDH1A2 expression as an early event in prostate cancer provides insight into the role of aberrant retinoid signaling in prostate cancer progression and highlights the importance of proper retinoid metabolism and signaling in the prevention of prostate cancer.

Disclosure statement

The authors do not have any conflicts of interest to disclose.

Acknowledgements

We would like to thank Karen Niederreither for providing us with wild type and ALDH1A2$^{-/-}$(Raldh2$^{-/-}$) embryos. We would also like to thank Mary Ng for technical assistance and members of the Gudas Laboratory for useful discussions. This work was supported in part by the Turobiner Kidney Cancer Research Fund (DMN) and NIH grant R01 CA097543 (LJG and DMN). Sue Ellen Touma was supported for a portion of this work from NCI T32 CA062948.

References

[1] Jemal A, Siegel R, Ward E, Hao Y, Xu J, Murray T, et al. Cancer statistics, 2008. CA Cancer J Clin 2008;58:71–96.
[2] Lasnitzki I, Goodman DS. Inhibition of the effects of methylcholanthrene on mouse prostate in organ culture by vitamin A and its analogs. Cancer Res 1974;34:1564–71.
[3] Chopra DP, Wilkoff LJ. Reversal by vitamin A analogues (retinoids) of hyperplasia induced by N-methyl-N′-nitro-N-nitrosoguanidine in mouse prostate organ cultures. J Natl Cancer Inst 1977;58:923–30.
[4] Chopra DP, Wilkoff LJ. Activity of retinoids against benzo(a)pyrene-induced hyperplasia in mouse prostate organ cultures. Eur J Cancer 1979;15:1417–23.
[5] Mongan NP, Gudas LJ. Diverse actions of retinoid receptors in cancer prevention and treatment. Differentiation 2007;75:853–70.
[6] Lotan R, Lotan Y. Retinoic acid receptor beta2 hypermethylation: implications for prostate cancer detection, prevention, and therapy. Clin Cancer Res 2004;10:3935–6.
[7] Nakayama T, Watanabe M, Yamanaka M, Hirokawa Y, Suzuki H, Ito H, et al. The role of epigenetic modifications in retinoic acid receptor beta2 gene expression in human prostate cancers. Lab Invest 2001;81:1049–57.
[8] Pili R, Kruszewski MP, Hager BW, Lantz J, Carducci MA. Combination of phenylbutyrate and 13-cis retinoic acid inhibits prostate tumor growth and angiogenesis. Cancer Res 2001;61:1477–85.
[9] Guo X, Knudsen BS, Peehl DM, Ruiz A, Bok D, Rando RR, et al. Retinol metabolism and lecithin:retinol acyltransferase levels are reduced in cultured human prostate cancer cells and tissue specimens. Cancer Res 2002;62:1654–61.
[10] Pasquali D, Thaller C, Eichele G. Abnormal level of retinoic acid in prostate cancer tissues. J Clin Endocrinol Metab 1996;81:2186–91.
[11] Kim H, Lapointe J, Kaygusuz G, Ong DE, Li C, van de Rijn M, et al. The retinoic acid synthesis gene ALDH1a2 is a candidate tumor suppressor in prostate cancer. Cancer Res 2005;65:8118–24.
[12] Duester G. Retinoic acid synthesis and signaling during early organogenesis. Cell 2008;134:921–31.
[13] Vasiliou V, Pappa A, Estey T. Role of human aldehyde dehydrogenases in endobiotic and xenobiotic metabolism. Drug Metab Rev 2004;36:279–99.
[14] Douville J, Beaulieu R, Balicki D. ALDH1 as a functional marker of cancer stem and progenitor cells. Stem Cells Dev 2008.
[15] Niederreither K, Dolle P. Retinoic acid in development: towards an integrated view. Nat Rev Genet 2008;9:541–53.
[16] Niederreither K, Subbarayan V, Dolle P, Chambon P. Embryonic retinoic acid synthesis is essential for early mouse post-implantation development. Nat Genet 1999;21:444–8.
[17] Trasino SE, Harrison EH, Wang TT. Androgen regulation of aldehyde dehydrogenase 1A3 (ALDH1A3) in the androgen-responsive human prostate cancer cell line LNCaP. Exp Biol Med (Maywood) 2007;232:762–71.
[18] Greenberg NM, DeMayo F, Finegold MJ, Medina D, Tilley WD, Aspinall JO, et al. Prostate cancer in a transgenic mouse. Proc Natl Acad Sci USA 1995;92:3439–43.
[19] Greenberg NM, DeMayo FJ, Sheppard PC, Barrios R, Lebovitz R, Finegold M, et al. The rat probasin gene promoter directs hormonally and developmentally regulated expression of a heterologous gene specifically to the prostate in transgenic mice. Mol Endocrinol 1994;8:230–9.
[20] Kaplan-Lefko PJ, Chen TM, Ittmann MM, Barrios RJ, Ayala GE, Huss WJ, et al. Pathobiology of autochthonous prostate cancer in a pre-clinical transgenic mouse model. Prostate 2003;55:219–37.
[21] Hurwitz AA, Foster BA, Allison JP, Greenberg NM, Kwon ED. The TRAMP mouse as a model for prostate cancer. Curr Protoc Immunol 2001 (Chapter 20: Unit 20.5).
[22] Sargeant AM, Rengel RC, Kulp SK, Klein RD, Clinton SK, Wang YC, et al. OSU-HDAC42, a histone deacetylase inhibitor, blocks prostate tumor progression in the transgenic adenocarcinoma of the mouse prostate model. Cancer Res 2008;68:3999–4009.
[23] Camoriano M, Kinney SR, Moser MT, Foster BA, Mohler JL, Trump DL, et al. Phenotype-specific CpG island methylation events in a murine model of prostate cancer. Cancer Res 2008;68:4173–82.
[24] Morey Kinney SR, Smiraglia DJ, James SR, Moser MT, Foster BA, Karpf AR. Stage-specific alterations of DNA methyltransferase expression, DNA hypermethylation, and DNA hypomethylation during prostate cancer progression in the transgenic adenocarcinoma of mouse prostate model. Mol Cancer Res 2008;6:1365–74.
[25] Raina K, Rajamanickam S, Singh RP, Deep G, Chittezhath M, Agarwal R. Stage-specific inhibitory effects and associated mechanisms of silibinin on tumor progression and metastasis in transgenic adenocarcinoma of the mouse prostate model. Cancer Res 2008;68:6822–30.
[26] Chung AC, Zhou S, Liao L, Tien JC, Greenberg NM, Xu J. Genetic ablation of the amplified-in-breast cancer 1 inhibits spontaneous prostate cancer progression in mice. Cancer Res 2007;67:5965–75.

[27] McCabe MT, Low JA, Daignault S, Imperiale MJ, Wojno KJ, Day ML. Inhibition of DNA methyltransferase activity prevents tumorigenesis in a mouse model of prostate cancer. Cancer Res 2006;66:385–92.
[28] Raina K, Rajamanickam S, Deep G, Singh M, Agarwal R, Agarwal C. Chemopreventive effects of oral gallic acid feeding on tumor growth and progression in TRAMP mice. Mol Cancer Ther 2008;7:1258–67.
[29] Raina K, Rajamanickam S, Singh RP, Agarwal R. Chemopreventive efficacy of inositol hexaphosphate against prostate tumor growth and progression in TRAMP mice. Clin Cancer Res 2008;14:3177–84.
[30] Singh SV, Powolny AA, Stan SD, Xiao D, Arlotti JA, Warin R, et al. Garlic constituent diallyl trisulfide prevents development of poorly differentiated prostate cancer and pulmonary metastasis multiplicity in TRAMP mice. Cancer Res 2008;68:9503–11.
[31] Singh RP, Raina K, Sharma G, Agarwal R. Silibinin inhibits established prostate tumor growth, progression, invasion, and metastasis and suppresses tumor angiogenesis and epithelial-mesenchymal transition in transgenic adenocarcinoma of the mouse prostate model mice. Clin Cancer Res 2008;14:7773–80.
[32] Bonorden MJ, Rogozina OP, Kluczny CM, Grossmann ME, Grande JP, Lokshin A, et al. Cross-sectional analysis of intermittent versus chronic caloric restriction in the TRAMP mouse. Prostate 2009;69:317–26.
[33] Adhami VM, Siddiqui IA, Sarfaraz S, Khwaja SI, Hafeez BB, Ahmad N, et al. Effective prostate cancer chemopreventive intervention with green tea polyphenols in the TRAMP model depends on the stage of the disease. Clin Cancer Res 2009;15:1947–53.
[34] Wang L, Bonorden MJ, Li GX, Lee HJ, Hu H, Zhang Y, et al. Methyl-selenium compounds inhibit prostate carcinogenesis in the transgenic adenocarcinoma of mouse prostate model with survival benefit. Cancer Prev Res (Phila PA) 2009;2:484–95.
[35] O'Mahony OA, Steinkamp MP, Albertelli MA, Brogley M, Rehman H, Robins DM. Profiling human androgen receptor mutations reveals treatment effects in a mouse model of prostate cancer. Mol Cancer Res 2008;6:1691–701.
[36] Venkateswaran V, Klotz LH, Ramani M, Sugar LM, Jacob LE, Nam RK, et al. A combination of micronutrients is beneficial in reducing the incidence of prostate cancer and increasing survival in the Lady transgenic model. Cancer Prev Res (Phila PA) 2009;2:473–83.
[37] Shappell SB, Thomas GV, Roberts RL, Herbert R, Ittmann MM, Rubin MA, et al. Prostate pathology of genetically engineered mice: definitions and classification. The consensus report from the Bar Harbor meeting of the mouse models of human cancer consortium prostate pathology committee. Cancer Res 2004;64:2270–305.
[38] Berquin IM, Min Y, Wu R, Wu H, Chen YQ. Expression signature of the mouse prostate. J Biol Chem 2005;280:36442–51.
[39] Deeb KK, Michalowska AM, Yoon CY, Krummey SM, Hoenerhoff MJ, Kavanaugh C, et al. Identification of an integrated SV40 T/t-antigen cancer signature in aggressive human breast, prostate, and lung carcinomas with poor prognosis. Cancer Res 2007;67:8065–80.
[40] Huss WJ, Lai L, Barrios RJ, Hirschi KK, Greenberg NM. Retinoic acid slows progression and promotes apoptosis of spontaneous prostate cancer. Prostate 2004;61:142–52.
[41] Gillespie RF, Gudas LJ. Retinoid regulated association of transcriptional coregulators and the polycomb group protein SUZ12 with the retinoic acid response elements of Hoxa1, RARbeta(2), and Cyp26A1 in F9 embryonal carcinoma cells. J Mol Biol 2007;372:298–316.
[42] Niederreither K, Vermot J, Schuhbaur B, Chambon P, Dolle P. Embryonic retinoic acid synthesis is required for forelimb growth and anteroposterior patterning in the mouse. Development 2002;129:3563–74.
[43] Haselbeck RJ, Hoffmann I, Duester G. Distinct functions for Aldh1 and Raldh2 in the control of ligand production for embryonic retinoid signaling pathways. Dev Genet 1999;25:353–64.
[44] Vernet N, Dennefeld C, Rochette-Egly C, Oulad-Abdelghani M, Chambon P, Ghyselinck NB, et al. Retinoic acid metabolism and signaling pathways in the adult and developing mouse testis. Endocrinology 2006;147:96–110.
[45] Everts HB, Sundberg JP, Ong DE. Immunolocalization of retinoic acid biosynthesis systems in selected sites in rat. Exp Cell Res 2005;308:309–19.
[46] Saleem M, Adhami VM, Ahmad N, Gupta S, Mukhtar H. Prognostic significance of metastasis-associated protein S100A4 (Mts1) in prostate cancer progression and chemoprevention regimens in an autochthonous mouse model. Clin Cancer Res 2005;11:147–53.
[47] Abate-Shen C, Shen MM. Molecular genetics of prostate cancer. Genes Dev 2000;14:2410–34.
[48] Cai K, Gudas LJ. Retinoic acid receptors and GATA transcription factors activate the transcription of the human lecithin:retinol acyltransferase gene. Int J Biochem Cell Biol 2009;41:546–53.
[49] Guo X, Nanus DM, Ruiz A, Rando RR, Bok D, Gudas LJ. Reduced levels of retinyl esters and vitamin A in human renal cancers. Cancer Res 2001;61:2774–81.
[50] Guo X, Ruiz A, Rando RR, Bok D, Gudas LJ. Esterification of all-trans-retinol in normal human epithelial cell strains and carcinoma lines from oral cavity, skin and breast: reduced expression of lecithin:retinol acyltransferase in carcinoma lines. Carcinogenesis 2000;21:1925–33.
[51] Poulin DL, DeCaprio JA. Is there a role for SV40 in human cancer? J Clin Oncol 2006;24:4356–65.
[52] Abate-Shen C, Shen MM. Mouse models of prostate carcinogenesis. Trends Genet 2002;18:S1–5.
[53] Sharma P, Schreiber-Agus N. Mouse models of prostate cancer. Oncogene 1999;18:5349–55.
[54] Peehl DM, Wong ST, Sellers RG, Jin S, Rhim JS. Loss of response to epidermal growth factor and retinoic acid accompanies the transformation of human prostatic epithelial cells to tumorigenicity with v-Ki-ras. Carcinogenesis 1997;18:1643–50.
[55] Ono Y, Fukuhara N, Yoshie O. TAL1 and LIM-only proteins synergistically induce retinaldehyde dehydrogenase 2 expression in T-cell acute lymphoblastic leukemia by acting as cofactors for GATA3. Mol Cell Biol 1998;18:6939–50.
[56] Rexer BN, Zheng WL, Ong DE. Retinoic acid biosynthesis by normal human breast epithelium is via aldehyde dehydrogenase 6, absent in MCF-7 cells. Cancer Res 2001;61:7065–70.
[57] Yamashita S, Tsujino Y, Moriguchi K, Tatematsu M, Ushijima T. Chemical genomic screening for methylation-silenced genes in gastric cancer cell lines using 5-aza-2'-deoxycytidine treatment and oligonucleotide microarray. Cancer Sci 2006;97:64–71.
[58] Ginestier C, Hur MH, Charafe-Jauffret E, Monville F, Dutcher J, Brown M, et al. ALDH1 is a marker of normal and malignant human mammary stem cells and a predictor of poor clinical outcome. Cell Stem Cell 2007;1:555–67.
[59] Tang DG, Patrawala L, Calhoun T, Bhatia B, Choy G, Schneider-Broussard R, et al. Prostate cancer stem/progenitor cells: identification, characterization, and implications. Mol Carcinog 2007;46:1–14.
[60] Lawson DA, Witte ON. Stem cells in prostate cancer initiation and progression. J Clin Invest 2007;117:2044–50.
[61] Takao T, Tsujimura A. Prostate stem cells: the niche and cell markers. Int J Urol 2008;15:289–94.
[62] Lawson DA, Xin L, Lukacs RU, Cheng D, Witte ON. Isolation and functional characterization of murine prostate stem cells. Proc Natl Acad Sci USA 2007;104:181–6.
[63] Oudes AJ, Campbell DS, Sorensen CM, Walashek LS, True LD, Liu AY. Transcriptomes of human prostate cells. BMC Genomics 2006;7:92.
[64] Mao GE, Reuter VE, Cordon-Cardo C, Dalbagni G, Scher HI, DeKernion JB, et al. Decreased retinoid X receptor-alpha protein expression in basal cells occurs in the early stage of human prostate cancer development. Cancer Epidemiol Biomarkers Prev 2004;13:383–90.
[65] Huss WJ, Maddison LA, Greenberg NM. Autochthonous mouse models for prostate cancer: past, present and future. Semin Cancer Biol 2001;11:245–60.
[66] Sprenger J, Lynn Fink J, Karunaratne S, Hanson K, Hamilton NA. Teasdale RD. LOCATE: a mammalian protein subcellular localization database. Nucleic Acids Res 2008;36:D230–3.
[67] King JC, Xu J, Wongvipat J, Hieronymus H, Carver BS, Leung DH, et al. Cooperativity of TMPRSS2-ERG with PI3-kinase pathway activation in prostate oncogenesis. Nat Genet 2009;41:524–6.